




Cite this: *Chem. Commun.*, 2023, 59, 2291

Received 2nd December 2022,  
Accepted 30th January 2023

DOI: 10.1039/d2cc06584c

rsc.li/chemcomm

# Synthesis of triarylborane-centered N-heterocyclic carbene cages with tunable photophysical properties†

Yi-Fan Zhang, Ya-Wen Zhang, Xin Li, Li-Ying Sun\* and Ying-Feng Han 

**Triarylborane-based discrete metal-carbene supramolecular cages  $[M_3(1)_2](PF_6)_3$  ( $M = Ag, Au$ ) were synthesized and characterized. The new hexacarbene assemblies show a significant solvatochromic effect in solvents of different polarity. Furthermore, the reversible fluoride binding property of  $[Au_3(1)_2](PF_6)_3$  was investigated by UV-vis absorption and fluorescence titrations. This work holds promise for future developments in the area of highly emissive and stimulus-responsive NHC-metal assemblies.**

Triarylborane (TAB)-involving functional materials has received significant attention over the past few years owing to their potential utility in numerous applications, such as catalysis,<sup>1</sup> organic optoelectronic materials,<sup>2</sup> anion sensors,<sup>3</sup> biological imaging<sup>4</sup> and frustrated Lewis pairs (FLPs).<sup>1,5</sup> Due to the inherent high reactivity of the boron center, its structural geometry and optical properties can be altered in the presence of suitable Lewis bases, such as fluoride ions.<sup>6</sup> Compared with a few examples of triarylborane-containing metal-organic frameworks (MOFs) that were described,<sup>7</sup> their applications in discrete organometallic supramolecular assemblies remain underexplored.<sup>8</sup>

During the past decade, continuous efforts have been made to construct supramolecular assemblies through coordination-driven self-assembly for different applications.<sup>9</sup> In this regard, functional ligands are attractive as building blocks to bring potential applications to the final structures. Among them, discrete supramolecular assemblies held together by metal-carbene bonds have attracted considerable attention. A variety of N-heterocyclic carbene (NHC) donor types have been used to construct supramolecular metal-NHC assemblies.<sup>10,11</sup> The obtained discrete NHC-based supramolecular systems have found wide applications in homogeneous catalysis,<sup>12</sup> metal

drugs,<sup>13</sup> and materials science.<sup>14</sup> Recent investigations on the exploration of metal-NHC-involving supramolecular assemblies have focused on their stimuli-responsive luminescence properties.<sup>15</sup> Given the excellent luminescence and photoelectronic properties of TAB, we became interested in synthesizing a new tris-NHC ligand featuring the TAB scaffold, which may bestow the cage with unique optoelectronic properties.

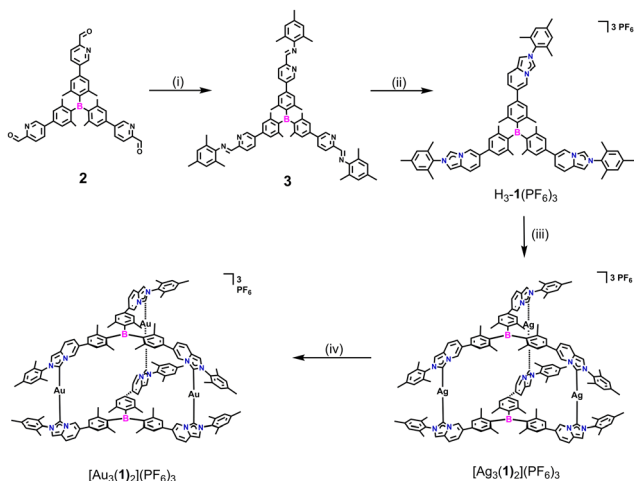
We herein present a new example of a discrete  $Ag^I$  hexacarbene supramolecular cage  $[Ag_3(1)_2](PF_6)_3$  containing Lewis acidic triarylborane-bridged NHC ligands. The assembly can be readily transformed to the corresponding  $Au^I$  analogue  $[Au_3(1)_2](PF_6)_3$ . Both metal-carbene supramolecular cages  $[Ag_3(1)_2](PF_6)_3$  and  $[Au_3(1)_2](PF_6)_3$  show solvent-induced luminescence response properties. The position of the corresponding luminescence band was found to be red shifted with an increase in solvent polarity. Notably, the boron centers of the metal carbene assemblies are prone to complex formation with Lewis bases and altering absorption and emission properties.

The palladium-catalyzed Suzuki cross-coupling of 5-bromo-2-pyridinecarboxaldehyde with boronate ester compounds provided borane-containing pyridinecarbaldehydes **2** (Scheme S1, Fig. S1 and S2, ESI†). Then, the imine condensation of **2** with 2,4,6-trimethylaniline in the presence of an acid catalyst led to the formation of compound **3**. Subsequently, the reaction of compound **3** with paraformaldehyde in the presence of 4 M HCl/1,4-dioxane solution, followed by anion exchange, yielded the desired triarylborane-bridged NHC precursor  $H_3-1(PF_6)_3$ . The formation of NHC precursor  $H_3-1(PF_6)_3$  was confirmed by nuclear magnetic resonance (NMR) spectroscopy ( $^1H$ ,  $^{13}C\{^1H\}$ , 2D NMR) and high resolution-electrospray ionization (HR-ESI) mass spectrometry (Fig. S3–S7, ESI†).

The reaction of TAB-bridged trisimidazo[1,5-*a*]pyridinium salt  $H_3-1(PF_6)_3$  with a slight excess of  $Ag_2O$  at 55 °C for 14 h afforded the trinuclear  $Ag^I$  hexacarbene  $[Ag_3(1)_2](PF_6)_3$  in an excellent yield of 96% (Scheme 1). The formation of hexacarbene metallocage  $[Ag_3(1)_2](PF_6)_3$  was initially verified by multinuclear NMR spectroscopy and HR-ESI mass spectrometry (Fig. S8–S14, ESI†). The  $^1H$  NMR spectrum of complex  $[Ag_3(1)_2](PF_6)_3$  featured

Key Laboratory of Synthetic and Natural Functional Molecule of the Ministry of Education, Xi'an Key Laboratory of Functional Supramolecular Structure and Materials, College of Chemistry and Materials Science, Northwest University, Xi'an 710127, P. R. China. E-mail: lysun@nwwu.edu.cn, yfhan@nwwu.edu.cn

† Electronic supplementary information (ESI) available: Experimental details, supporting figures and tables. CCDC 2167062. For ESI and crystallographic data in CIF or other electronic format see DOI: <https://doi.org/10.1039/d2cc06584c>



**Scheme 1** Synthesis of the triarylborane-bridged NHC precursor  $H_3-1(PF_6)_3$  and trinuclear hexacarbene complexes. (i) 2,4,6-Trimethylaniline,  $CH_3COOH$ ,  $CHCl_3/EtOH$ , reflux; (ii) (a) paraformaldehyde,  $HCl$ ,  $25^\circ C$ ; (b)  $NH_4PF_6$ ,  $MeOH$ ,  $25^\circ C$ , yield 51%; (iii)  $Ag_2O$ ,  $CH_3CN$ ,  $55^\circ C$ , yield 96%; (iv)  $AuCl(THT)$ ,  $CH_3CN$ ,  $25^\circ C$ , yield 83%.

no resonance for  $H_1$  protons of the imidazo[1,5-*a*]pyridinium group, which was previously observed for  $H_3-1(PF_6)_3$  at  $\delta = 9.15$  ppm in  $CD_3CN$  (Fig. 1a and b). The peaks in the  $^1H$  NMR spectrum of  $[Ag_3(1)_2](PF_6)_3$  showed pronounced shifts with respect to those of the NHC precursor  $H_3-1(PF_6)_3$ . Specifically, the resonance of  $H_{11}$  protons of  $[Ag_3(1)_2](PF_6)_3$  was downfield shifted, while the other protons of the imidazo[1,5-*a*]pyridinium group were upfield shifted as compared to the NHC precursor. Additionally, the  $^{13}C\{^1H\}$  NMR spectrum of  $[Ag_3(1)_2](PF_6)_3$  displayed the typical resonance of a carbene carbon atom at  $\delta = 175.8$  ppm. The formation of the complex  $[Ag_3(1)_2](PF_6)_3$  was further confirmed by HR-ESI mass spectrometry, by the highest intensity peak at  $m/z = 793.9169$  (calcd for  $[Ag_3(1)_2]^{3+}$  793.9517) (Fig. 1c).

Stirring an acetonitrile solution of  $[Ag_3(1)_2](PF_6)_3$  with three equivalents of  $[AuCl(THT)]$  (THT = tetrahydrothiophene) for

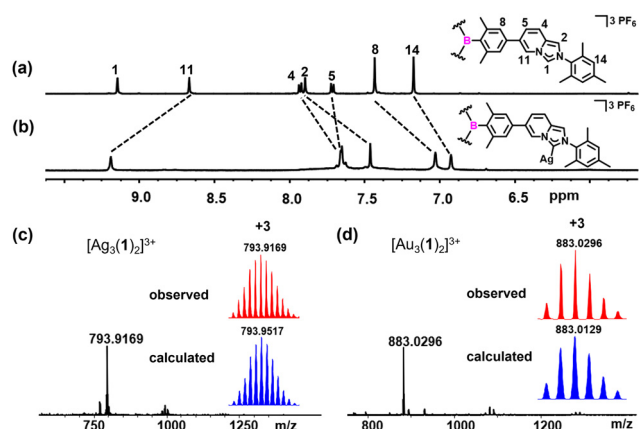


**Fig. 1** Sections of the  $^1H$  NMR spectra (600 MHz,  $CD_3CN$ ) of (a)  $H_3-1(PF_6)_3$  and (b)  $[Ag_3(1)_2](PF_6)_3$ . The HR-ESI mass spectra of (c)  $[Ag_3(1)_2](PF_6)_3$  and (d)  $[Au_3(1)_2](PF_6)_3$  (experimental in red, calculated in blue).

24 h at ambient temperature gave exclusively the trinuclear  $Au^I$  hexacarbene complex  $[Au_3(1)_2](PF_6)_3$  in 83% yield. All the three  $Ag^I$  in  $[Ag_3(1)_2](PF_6)_3$  can be substituted by  $Au^I$  to give the homonuclear complex  $[Au_3(1)_2](PF_6)_3$  without destroying the three-dimensional metallocsupramolecular assembly. The conversion of the silver complex to the gold one was characterized by  $^1H$ ,  $^{13}C\{^1H\}$ ,  $^{19}F$ ,  $^{31}P$ , and 2D NMR spectroscopy and HR-ESI mass spectrometry (Fig. S15–S20, ESI $^\dagger$ ). HR-ESI mass spectrometry of  $[Au_3(1)_2](PF_6)_3$  showed the highest intensity peak at  $m/z = 883.0296$  (calcd for  $[Au_3(1)_2]^{3+}$  883.0129) (Fig. 1d).

In addition, single-crystal X-ray diffraction unambiguously confirmed the molecular structure of the complex  $[Ag_3(1)_2](PF_6)_3$ . Crystals suitable for X-ray diffraction were grown by the slow diffusion of diethyl ether into a saturated acetonitrile solution at room temperature. Complex  $[Ag_3(1)_2](PF_6)_3$  crystallizes in the monoclinic  $C2/c$  space group and the central B atoms have an ideal trigonal-planar geometry with the sum of the C8-B-C5, C5-B-C9, and C8-B-C9 angles being  $359.9^\circ$  (Fig. 2a). As shown in Fig. 2b, the distance between the two boron atoms was measured to be  $7.102(5)$  Å. Due to the steric repulsion between the six *ortho*-methyl groups around the boron atom, tricoordinate central boron atoms formed a propeller-like structure, which prevented  $\pi$ -stacking interaction between the two triarylborane units. Indeed, complex  $[Ag_3(1)_2](PF_6)_3$  exists as a racemic mixture in solution and crystallizes as a racemic modification of the *P* and *M* enantiomers (Fig. S21, ESI $^\dagger$ ).<sup>16</sup> Furthermore, weak intermolecular C-H... $\pi$  interactions were found between the *N*-mesityl group and the imidazo[1,5-*a*]pyridine ring in the molecular stacking diagram in which the separation between the point-centroids was  $3.497(2)$  Å (Fig. S23, ESI $^\dagger$ ). Moreover, the bond length and the bond angle parameters of each component of the complex cation

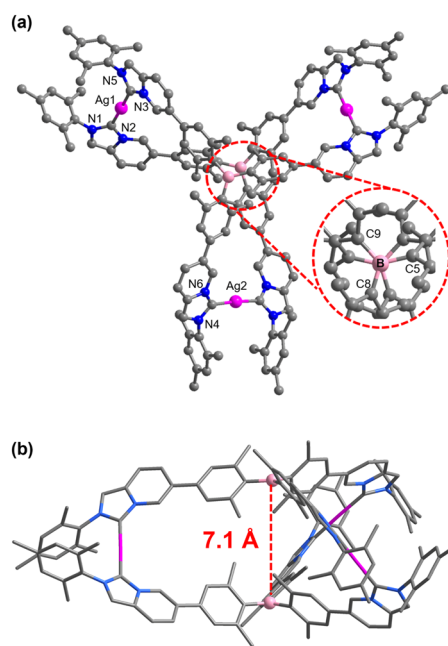


**Fig. 2** Molecular structure of the trication  $[Ag_3(1)_2]^{3+}$  in  $[Ag_3(1)_2](PF_6)_3$ : (a) top view, (b) side view. Hydrogen atoms and counteranions are omitted for clarity; color code: B, pink; Ag, violet; N, blue; C, gray.



Fig. 3 (a) The UV-vis absorption and (b) normalized emission spectra of  $H_3-1(PF_6)_3$ ,  $[Ag_3(1)_2](PF_6)_3$ , and  $[Au_3(1)_2](PF_6)_3$  in acetonitrile solution ( $\lambda_{ex} = 330$  nm,  $c = 10^{-5}$  M, and  $T = 298$  K).

$[Ag_3(1)_2]^{3+}$  were measured (Ag–C<sub>NHC</sub> bond lengths, 2.036(10)–2.082(10) Å, C<sub>NHC</sub>–Ag–C<sub>NHC</sub> bond angles, 176.4(5)°–178.2(4)°, and N–C<sub>NHC</sub>–N bond angles, 101.1(8)°–104.0(8)°). These parameters fall within the range previously reported for related Ag<sup>I</sup> polycarbene assemblies.<sup>17</sup>

Since triarylboranes are promising fluorescent skeleton molecules,<sup>18</sup> we further investigated the optical properties of the NHC precursor and its Ag<sup>I</sup> and Au<sup>I</sup> complexes. The UV-vis absorption spectra of the NHC precursor and the trinuclear hexacarbene metal complexes showed similar types of absorption curves in the range of 220–400 nm (Fig. 3a). The lower energy band results from the imidazo[1,5-*a*]pyridinium groups to boron intramolecular charge transfer (ICT) and the higher energy band can be attributed to the boron aryl center  $\pi$ – $\pi^*$  transitions.<sup>19</sup> Upon excitation at 330 nm, the NHC precursor  $H_3-1(PF_6)_3$  and trinuclear hexacarbene complexes showed different emission curves in acetonitrile solution, as  $\lambda_{em} = 418$  nm for  $H_3-1(PF_6)_3$ , 487 nm for  $[Ag_3(1)_2](PF_6)_3$  and 478 nm for  $[Au_3(1)_2](PF_6)_3$ . A red-shift of the emission maximum was observed for the NHC precursor upon metalation (Fig. 3b). The absolute fluorescence quantum yields determined for the solutions of  $H_3-1(PF_6)_3$ ,  $[Ag_3(1)_2](PF_6)_3$ , and  $[Au_3(1)_2](PF_6)_3$  were 21.76, 19.19, and 1.46%, respectively. All the photophysical data are summarized in Table S2 (ESI†).

As illustrated in Fig. 4, the fluorescence emission spectra of the hexacarbene complexes in both polar (*e.g.*, DMSO, DMF, and



Fig. 4 The normalized fluorescence emission spectra of (a)  $[Ag_3(1)_2](PF_6)_3$  and (b)  $[Au_3(1)_2](PF_6)_3$  in various solvents ( $\lambda_{ex} = 330$  nm,  $c = 10^{-5}$  M, and  $T = 298$  K). Photographs of (c)  $[Ag_3(1)_2](PF_6)_3$  and (d)  $[Au_3(1)_2](PF_6)_3$  in various solvents under UV light.

MeCN) and nonpolar solvents (*e.g.*, DCE, DCM, and THF) were highly tunable over a broad spectrum from 450 nm to 550 nm. The emission bands were red-shifted with an increase in the solvent polarity, showing the characteristics of highly solvent-dependent emission, donor–acceptor charge transfer, and a highly polarized excited state (Fig. S24 and S25, ESI†).<sup>20</sup> To gain an insight into the emission characteristics of the NHC precursor and the trinuclear hexacarbene complexes, DFT theoretical calculations were used to reveal their electronic structures and electron transition orbits (Fig. S26, ESI†). The HOMO and LUMO energy levels of  $H_3-1(PF_6)_3$  are –11.24 and –7.38 eV, respectively. The HOMO energy levels of the complexes  $[Ag_3(1)_2](PF_6)_3$  and  $[Au_3(1)_2](PF_6)_3$  are –9.86 eV, while the LUMO energy levels of the complexes  $[Ag_3(1)_2](PF_6)_3$  and  $[Au_3(1)_2](PF_6)_3$  are –6.39 and –6.43 eV, respectively. The HOMO is mainly localized in the imidazo[1,5-*a*]pyridine group, while the LUMO is in the triarylborane group. This finding further suggests that the low-energy emission is mainly due to the ICT transfer between triarylborane ( $\pi$ ) and boron-bound phenyl rings ( $\pi^*$ ).

Considering that the interaction between the ligands and gold atoms further increases the stability of the complex, we use the trinuclear hexacarbene cage  $[Au_3(1)_2](PF_6)_3$  in fluoride ion sensing that was monitored by absorption and emission studies. In the UV-vis absorption spectra, the complex  $[Au_3(1)_2](PF_6)_3$  featured a broad low-energy absorption band centered at 360 nm, which was gradually quenched upon the addition of an increasing amount of fluoride ions, and the peak at 265 nm also decreased (Fig. 5a). The absorption spectral change can be assigned primarily to the binding of  $F^-$  with the boron center.<sup>21</sup> This corresponding change can be rationalized as a result of the interruption of the  $\pi$ -conjugation extending through the vacant p-orbital of the boron atom by forming the corresponding fluoroborate.<sup>22</sup> In the fluorescence titration, the emission band of the complex  $[Au_3(1)_2](PF_6)_3$  at 478 nm was quenched by the addition of fluoride ions (Fig. 5b). This finding indicated that the



Fig. 5 (a) The UV-vis absorption and (b) fluorescence emission spectra of  $[Au_3(1)_2](PF_6)_3$  with TBAF (tetrabutylammonium fluoride). (c) The UV-vis absorption and (d) fluorescence emission spectra of  $[Au_3(1)_2](PF_6)_3$  with  $BF_3 \cdot Et_2O$  in the presence of 2 equivalents of TBAF ( $CH_3CN$ ,  $\lambda_{ex} = 330$  nm,  $c = 10^{-5}$  M, and  $T = 298$  K).



low energy absorption in  $[\text{Au}_3(1)_2](\text{PF}_6)_3$  was mainly assignable to the triarylborane-centered  $\pi \rightarrow p_\pi(\text{B})$  charge transfer transition.<sup>23</sup> According to previous reports,<sup>8</sup> we guessed that the cage and fluoride ions were bound in a molar ratio of 1 : 2, and a nonlinear least-squares curve fitting procedure and the conclusion of the conducted Job's plot experiments provided further evidence (Fig. S27 and S28, ESI†).

Subsequently, the reversibility of fluoride binding in the complex  $[\text{Au}_3(1)_2](\text{PF}_6)_3$  was studied using  $\text{BF}_3 \cdot \text{Et}_2\text{O}$  as an external Lewis acid. Both the UV-vis absorption and fluorescence emission spectra of  $[\text{Au}_3(1)_2](\text{PF}_6)_3$  showed reversible processes (Fig. 5c and d), which demonstrated that the  $\text{Au}^{\text{I}}$  hexacarbene cage was stable in the presence of excess fluoride ions.

In summary, we have successfully synthesized the trigonal prismatic  $\text{Ag}^{\text{I}}$  and  $\text{Au}^{\text{I}}$  hexacarbene cages by a metal-controlled self-assembly approach from triarylborane-based tris-NHC ligands and silver or gold ions. The molecular structure of  $[\text{Ag}_3(1)_2](\text{PF}_6)_3$  was confirmed by X-ray crystallography. Notably, the fluorescence spectra of the trinuclear hexacarbene complexes show some degree of dependence on the solvent polarity. In particular, the fluoride binding and removal properties of  $[\text{Au}_3(1)_2](\text{PF}_6)_3$  were investigated by the UV-vis absorption and fluorescence titrations. The results showed that the triarylborane-based cage had a strong fluorine-binding ability. The results of this study not only provided insight into the design principles of metal coordination-driven self-assembly but also demonstrate the ON/OFF and OFF/OFF fluorescence switching in the presence and absence of fluoride ions, opening a new route for the development of chemical sensors.

This work was supported by the National Natural Science Fund for Distinguished Young Scholars of China (No. 22025107), the National Youth Top-notch Talent Support Program of China and the National Natural Science Foundation of China (22101225), Natural Science Foundation of Shaanxi Province (2021JQ432), Xi'an Key Laboratory of Functional Supramolecular Structure and Materials, and the FM&EM International Joint Laboratory of Northwest University.

## Conflicts of interest

There are no conflicts to declare.

## Notes and references

- J. L. Carden, A. Dasgupta and R. L. Melen, *Chem. Soc. Rev.*, 2020, **49**, 1706–1725.
- M. Elbing and G. C. Bazan, *Angew. Chem., Int. Ed.*, 2008, **47**, 834–838.
- (a) C. A. Swamy and P. P. Thilagar, *Inorg. Chem.*, 2014, **53**, 2776–2786; (b) M.-S. Yuan, X. Du, Z. Liu, T. Li, W. Wang, E. V. Anslyn and J. Wang, *Chem. – Eur. J.*, 2018, **24**, 9211–9216.
- S. M. Berger and T. B. Marder, *Mater. Horiz.*, 2022, **9**, 112–120.
- D. W. Stephan, *J. Am. Chem. Soc.*, 2015, **137**, 10018–10032.
- (a) Z. M. Hudson and S. Wang, *Acc. Chem. Res.*, 2009, **42**, 1584–1596; (b) Q. Xia, J. Zhang, X. Chen, C. Cheng, D. Chu, X. Tang, H. Li and Y. Cui, *Coord. Chem. Rev.*, 2021, **435**, 213783.
- (a) Y. Liu, X. Xu, Q. Xia, G. Yuan, Q. He and Y. Cui, *Chem. Commun.*, 2010, **46**, 2608–2610; (b) S. Shyshkanov, T. N. Nguyen, F. M. Ebrahim, K. C. Stylianou and P. J. Dyson, *Angew. Chem., Int. Ed.*, 2019, **58**, 5371–5375; (c) T. N. Nguyen, I. M. Harreschou, J.-H. Lee, K. C. Stylianou and D. W. Stephan, *Chem. Commun.*, 2020, **56**, 9600–9603; (d) B. A. Blight, R. Guillet-Nicolas, F. Kleitz, R.-Y. Wang and S. Wang, *Inorg. Chem.*, 2013, **52**, 1673–1675; (e) F. M. Ebrahim, T. N. Nguyen, S. Shyshkanov, A. Gladysiak, P. Favre, A. Zacharia, G. Itskos, P. J. Dyson and K. C. Stylianou, *J. Am. Chem. Soc.*, 2019, **141**, 3052–3058.
- (a) N. Mihara, T. K. Ronson and J. R. Nitschke, *Angew. Chem., Int. Ed.*, 2019, **58**, 12497–12501; (b) J. Y. Ryu, J. M. Lee, N. V. Nghia, K. M. Lee, S. Lee, M. H. Lee, P. J. Stang and J. Lee, *Inorg. Chem.*, 2018, **57**, 11696–11703.
- (a) Z. Wang, L. He, B. Liu, L.-P. Zhou, L.-X. Cai, S.-J. Hu, X.-Z. Li, Z. Li, T. Chen, X. Li and Q.-F. Sun, *J. Am. Chem. Soc.*, 2020, **142**, 16409–16419; (b) P.-F. Cui, Y.-J. Lin, Z.-H. Li and G.-X. Jin, *J. Am. Chem. Soc.*, 2020, **142**, 8532–8538; (c) P.-F. Cui, X.-R. Liu, Y.-J. Lin, Z.-H. Li and G.-X. Jin, *J. Am. Chem. Soc.*, 2022, **144**, 6558–6565; (d) X. Gao, Z. Cui, Y.-R. Shen, D. Liu, Y.-J. Lin and G.-X. Jin, *J. Am. Chem. Soc.*, 2021, **143**, 17833–17842.
- (a) P. J. Altmann and A. Pöthig, *Angew. Chem., Int. Ed.*, 2017, **56**, 15733–15736; (b) P. J. Altmann and A. Pöthig, *J. Am. Chem. Soc.*, 2016, **138**, 13171–13174; (c) L.-L. Ma, Y. Li, X. Li, L. Zhang, L.-Y. Sun and Y.-F. Han, *Angew. Chem., Int. Ed.*, 2022, **61**, e202208376.
- (a) N. Sinha, L. Stegemann, T. T. Y. Tan, N. L. Doltsinis, C. A. Strassert and F. E. Hahn, *Angew. Chem., Int. Ed.*, 2017, **56**, 2785–2789; (b) N. Sinha and F. E. Hahn, *Acc. Chem. Res.*, 2017, **50**, 2167–2184; (c) M.-M. Gan, J.-Q. Liu, L. Zhang, Y.-Y. Wang, F. E. Hahn and Y.-F. Han, *Chem. Rev.*, 2018, **118**, 9587–9641; (d) S. Ibáñez, M. Poyatos and E. Peris, *Acc. Chem. Res.*, 2020, **53**, 1401–1413; (e) Z.-E. Zhang, Y.-Y. An, B. Zheng, J.-P. Chang and Y.-F. Han, *Sci. China: Chem.*, 2021, **64**, 1177–1183; (f) X.-X. Liu, Y. Li, X. Li, F. E. Hahn and Y.-F. Han, *Sci. China: Chem.*, 2021, **64**, 1709–1715; (g) R. C. Nishad, S. Kumar and A. Rit, *Angew. Chem., Int. Ed.*, 2022, **61**, e202206788.
- (a) E. Peris, *Chem. Rev.*, 2018, **118**, 9988–10031; (b) T. Liu, S. Bai, L. Zhang, F. E. Hahn and Y.-F. Han, *Natl. Sci. Rev.*, 2022, **9**, nwac067.
- W. Liu and R. Gust, *Coord. Chem. Rev.*, 2016, **329**, 191–213.
- (a) A. V. Zhukhovitskiy, M. J. MacLeod and J. A. Johnson, *Chem. Rev.*, 2015, **115**, 11503–11532; (b) R. Zhong, A. C. Lindhorst, F. J. Groche and F. E. Kühn, *Chem. Rev.*, 2017, **117**, 1970–2058; (c) R. Visbal and M. C. Gimeno, *Chem. Soc. Rev.*, 2014, **43**, 3551–3574.
- (a) Y. Li, T. Yang, N. Li, S. Bai, X. Li, L.-L. Ma, K. Wang, Y. Zhang and Y.-F. Han, *CCS Chem.*, 2022, **4**, 732–743; (b) Y. Li, Y.-Y. An, J.-Z. Fan, X.-X. Liu, X. Li, F. E. Hahn, Y.-Y. Wang and Y.-F. Han, *Angew. Chem., Int. Ed.*, 2020, **59**, 10073–10080.
- Y. Liu, X. Xu, F. Zheng and Y. Cui, *Angew. Chem., Int. Ed.*, 2008, **47**, 4538–4541.
- (a) A. Rit, T. Pape and F. E. Hahn, *J. Am. Chem. Soc.*, 2010, **132**, 4572–4573; (b) Y.-F. Han, G.-X. Jin and F. E. Hahn, *J. Am. Chem. Soc.*, 2013, **135**, 9263–9266.
- (a) K. Parab, K. Venkatasubbaiah and F. Jäkle, *J. Am. Chem. Soc.*, 2006, **128**, 12879–12885; (b) J. Liu, S. Zhang, C. Zhang, J. Dong, C. Shen, J. Zhu, H. Xu, M. Fu, G. Yang and X. Zhang, *Chem. Commun.*, 2017, **53**, 11476–11479; (c) L. Ji, S. Griesbeck and T. B. Marder, *Chem. Sci.*, 2017, **8**, 846–863; (d) S. Pagidi, N. K. Kalluvettukuzhy and P. Thilagar, *Organometallics*, 2018, **37**, 1900–1909.
- (a) B. H. Choi, J. H. Lee, H. Hwang, K. M. Lee and M. H. Park, *Organometallics*, 2016, **35**, 1771–1777; (b) P. Sudhakar, K. K. Neena and P. Thilagar, *J. Mater. Chem. C*, 2017, **5**, 6537–6546.
- S. Pagidi, N. K. Kalluvettukuzhy and P. Thilagar, *Inorg. Chem.*, 2020, **59**, 3142–3151.
- (a) F. Cheng, E. M. Bonder and F. Jäkle, *J. Am. Chem. Soc.*, 2013, **135**, 17286–17289; (b) S. W. Kwak, H. Kwon, J. H. Lee, H. Hwang, M. Kim, Y. Chung, Y. Kim, K. M. Lee and M. H. Park, *Dalton Trans.*, 2018, **47**, 5310–5317.
- (a) S. Yamaguchi and A. Wakamiya, *Pure Appl. Chem.*, 2006, **78**, 1413–1424; (b) Z. Zhou, A. Wakamiya, T. Kushida and S. Yamaguchi, *J. Am. Chem. Soc.*, 2012, **134**, 4529–4532.
- H. Lee, S. Jana, J. Kim, S. U. Lee and M. H. Lee, *Inorg. Chem.*, 2020, **59**, 1414–1423.